Available online at www.sciencedirect.com

ScienceDirect

Geochimica et Cosmochimica Acta 226 (2018) 18–35

Geochimica et Cosmochimica Acta

www.elsevier.com/locate/gca

Calcium isotope systematics at hydrothermal conditions: Mid-ocean ridge vent fluids and experiments in the $CaSO_4$-NaCl-H_2O system

Peter P. Scheuermann [a,*], Drew D. Syverson [a,b], John A. Higgins [c], Nicholas J. Pester [d], William E. Seyfried Jr. [a]

[a] University of Minnesota, Department of Earth Sciences, 116 Church St. SE, Minneapolis, MN 55455, United States
[b] Yale University, Department of Geology and Geophysics, New Haven, CT 06520, United States
[c] Princeton University, Department of Geosciences, Guyot Hall, Washington Road, Princeton, NJ 08544, United States
[d] Lawrence Berkeley National Laboratory, Earth Sciences Division, One Cyclotron Road, Berkeley, CA 94720, United States

Received 7 July 2017; accepted in revised form 19 January 2018; available online 13 February 2018

Abstract

Two sets of hydrothermal experiments were performed to explore Ca isotope fractionation and exchange rates at hydrothermal conditions (410–450 °C, 31.0–50.0 MPa). The first set of experiments determined the magnitude of vapor-liquid Ca isotope fractionation and anhydrite solubility in the $CaSO_4$-NaCl-H_2O system. The data indicate no statistical difference between the Ca isotopic composition of coexisting vapor and liquid. The second set of experiments utilized an anomalous ^{43}Ca spike to determine the rate of Ca exchange between fluid and anhydrite as a function of total dissolved Ca concentration. Results show that the rate of exchange increases with dissolved Ca concentrations (12–23 mM/kg), but no change in exchange rate is observed when the Ca concentration increases from 23 to 44 mM/kg Ca. 74–142 days are required to achieve 90% anhydrite-fluid Ca isotope exchange at the conditions investigated, while only several hours are necessary for vapor-liquid isotopic equilibrium. The lack of vapor-liquid Ca isotope fractionation in our experiments is consistent with $\delta^{44}Ca$ of mid-ocean ridge hydrothermal vent fluids that remain constant, regardless of chlorinity. Moreover, the narrow range of end member fluid $\delta^{44}Ca$, −0.98 to −1.13‰ (SW), is largely indistinguishable from MORB $\delta^{44}Ca$, suggesting that neither phase separation nor fluid-rock interactions at depth significantly fractionate Ca isotopes in modern high-temperature mid-ocean ridge hydrothermal systems.

Keywords: Mid-ocean ridge; Hydrothermal; Calcium isotopes; Anhydrite; Phase separation; Isotope exchange

1. INTRODUCTION

High temperature hydrothermal systems at mid-ocean ridges play an important role in determining the chemical and isotopic composition of seawater on geologic time-scales. In particular, these systems represent an important sink of seawater Ca to the mantle and source of mantle Ca to seawater. It has been hypothesized that variations in the rate of seafloor spreading and associated fluxes of seawater through high temperature mid-ocean ridge (MOR) hydrothermal systems have produced large changes in the major element chemistry of seawater (Hardie, 1996; Holland, 2005). A better understanding of the chemical and isotopic fluxes of Ca through axial vent systems has important ramifications for understanding Ca cycling in modern and ancient oceans (De La Rocha and DePaolo, 2000; Fantle, 2010; Antonelli et al., 2017).

* Corresponding author.
E-mail address: scheu101@umn.edu (P.P. Scheuermann).

https://doi.org/10.1016/j.gca.2018.01.028
0016-7037/

As seawater is heated in the recharge zone of axial vent systems, anhydrite ($CaSO_4$) precipitation occurs at temperatures exceeding 140 °C (Bischoff and Seyfried, 1978). During discharge of fluids on and near the seafloor at deep sea vents, mixing of SO_4 rich seawater and Ca rich hydrothermal fluid also causes anhydrite to precipitate (Tivey et al., 1995). There is also evidence from drill cores, sulfur isotope analysis and theoretical calculations that anhydrite exists near the base of hydrothermal circulation cells (Ono et al., 2007; Alt et al., 2010; McDermott, 2015). Given its widespread occurrence in marine hydrothermal systems, anhydrite is thought to have significant effects on both the hydrogeology of the ocean crust, through porosity reduction during precipitation (Sleep, 1991; Lowell et al., 2003), and redox chemistry of high-temperature vent fluids (Seyfried and Ding, 1995).

In addition to fluid-rock interactions, phase separation of hydrothermal fluid influences the chemical and isotopic flux of dissolved components to the seafloor (Von Damm, 1995, 2004). Elemental partitioning and isotopic fractionation at pressure-temperature conditions representative of natural hydrothermal systems have been previously studied experimentally for a range of transition metals, alkali and alkali earth elements (Berndt et al., 1996; Heinrich et al., 1999; Liebscher et al., 2005, 2006; Foustoukos and Seyfried, 2007b; Rempel et al., 2012; Pokrovski et al., 2013; Syverson et al., 2014; Pester et al., 2015). These studies provide the solubility and isotopic constraints necessary to interpret field data taken from two-phase submarine (Foustoukos et al., 2004; Rouxel et al., 2004, 2008) and subaerial (Simmons and Brown, 2006; Hardardóttir et al., 2009) hydrothermal systems, while also serving as independent checks on first principle calculations of isotopic fractionation (Anbar et al., 2005; Chialvo and Horita, 2009; Rustad et al., 2010). Additionally, isotopic studies of two-phase fluid systems are useful to identify changes in aqueous speciation between vapor and liquid, given that, for many elements, the bonding and coordination environment in either phase often prefers one isotope relative to others (Liebscher et al., 2005, 2006; Rempel et al., 2012; Syverson et al., 2014). For example, Syverson et al. (2014) proposed that Fe isotope fractionation was caused by two distinct Fe species, $[FeCl_2(H_2O)_2]^0$ and $[FeCl_4]^{2-}$, coexisting in the vapor and liquid, respectively. With increasing departure from the two-phase boundary of the NaCl-H_2O system, the magnitude of Fe isotope fractionation increased as the two species presumably became more abundant in their respective phases.

In this study we present results from laboratory experiments of the $CaSO_4$-NaCl-H_2O system and natural samples from modern seafloor hydrothermal systems to determine: (1) the extent to which Ca isotopes fractionate during phase separation; (2) rates of anhydrite recrystallization as a function of dissolved Ca concentration; and, (3) the Ca isotopic composition of mid-ocean ridge hydrothermal fluids from two basalt-hosted vent systems. These data provide further constraints on the reactions responsible for Ca cycling within modern seafloor hydrothermal systems and a foundation for exploring how these systems may have changed over Earth history.

2. METHODS

2.1. Phase separation experiments

Phase separation experiments (experiments 1 and 2) were conducted at 420 and 450 °C between 31.0 and 46.0 MPa in flexible gold reaction cells (Seyfried et al., 1987). These temperatures and pressures were chosen in order to study Ca isotopic behavior at conditions representative of fast-spreading ridges at steady-state hydrothermal conditions (Foustoukos and Seyfried, 2007a; Fontaine et al., 2009; Pester et al., 2011, 2014). The NaCl composition of the two fluids at these conditions are well known (Sourirajan and Kennedy, 1962; Bischoff and Pitzer, 1989; Driesner, 2007; Driesner and Heinrich, 2007), and thus serve as a check for the results of the experiments presented here.

Experiments were performed isothermally and single-phase fluid samples were taken before decompressing to pressures within the vapor-liquid region. A Teledyne ISCO syringe pump remained connected to the pressurizing fluid that surrounds the gold reaction cell to control pressure within ±0.5 MPa of the reported value (see Fig. 1 in Berndt et al., 1996). For these experiments, the reaction time at a specific pressure-temperature condition ranged between 12 and 72.25 h, with the majority falling between 18 and 28 h. The sampling rate, manually controlled by a titanium-regulating valve, was maintained sufficiently low (<1 mL/min) so as to maintain steady-state conditions. As a result, neither temperature nor pressure changed by more than 1 °C or 0.1 MPa during sampling.

Given the volume limits of the gold reaction cell, care was taken to maintain the total volume of the system (vapor + liquid) below the maximum volume of the cell, 72 cm^3. The volume and mass fraction of each phase was calculated by mass balance on the bulk mole fraction of NaCl in the system. The NaCl composition of the two phases and the densities were taken from the literature (Driesner, 2007; Driesner and Heinrich, 2007).

Vapor and liquid samples were taken intermittently during experiment 1. Only samples of vapor were taken during the first decompression in experiment 2. The pressure was then increased to near the two-phase boundary and additional stock solution (Table 1) was added to the gold reaction cell with a second Teledyne ISCO syringe pump. The gold reaction cell and supporting pressure vessel were then rotated to allow for sampling of the liquid phase during a second stage of decompression.

All stock solutions (phase separation and isotope exchange experiments) were prepared with reagent grade salts and 18.2 mΩ deionized water. Samples were taken in clean pre-weighed luer lock syringes, weighed approximately 2 g and were separated into aliquots for total dissolved chemistry, Ca isotope and pH measurements. Before each sample, 0.3 g of fluid were removed and discarded to ensure that the fluid sample comes directly from the gold cell and not residual fluid in the capillary exit line. At the end of each experiment, 0.45 μm pore size nylon filters were used to filter anhydrite from solution and were dried for 24 h at 60 °C.

Table 1
Chemical composition of phase separation experiments.

	Pressure (MPa)	Phase	Na (mM)	Cl (mM)	Ca (mM)	SO_4 (μM)	$pH_{25°C}$
Experiment 1 420 °C							
Stock solution			563.14	603.2	44.0	22,600	5.63
1.3	37.5	1 phase	559.7	580.5	19.5	BDL	5.84
1.4	32.5	Vapor	160.6	156.7	2.5	BDL	4.54
1.5	32.5	Liquid	1859.0	2054.9	80.3	415	7.54
1.6	31.7	Liquid	2183.0	2393.7	88.1	612	6.26
1.7	31.7	Vapor	121.9	132.0	1.7	BDL	4.47
Experiment 2 450 °C							
Stock solution			927.2	1052.9	81.1	19,800	5.45
2.1	46.0	1 phase	886.5	994.1	58.2	169	4.74
2.2	40.5	Vapor	315.1	328.5	8.1	290	3.51
2.3	39.5	Vapor	213.6	222.0	3.4	225	3.4
2.4	38.5	Vapor	149.7	152.9	1.4	BDL	3.4
2.5	37.5	Vapor	111.1	111.9	0.7	BDL	3.43
2.6	40.5	Liquid	2987.9	3161.7	86.3	1600	5.87
2.7	39.5	Liquid	3127.1	3310.0	85.9	1700	6.29
2.8	38.5	Liquid	3555.0	3746.2	98.1	2500	6.5
2.9	37.5	Liquid	4029.8	4217.9	110.5	3700	7.15

mM = mmol/kg solution.
μM = μmol/kg solution.
BDL = below detection limit.

2.2. Isotope exchange experiments

Isotope exchange experiments (A, B and C) were performed at 410 °C, 50.0 MPa also in a flexible gold cell reactor. The fluid phase in all three experiments simulated mid-ocean ridge hydrothermal fluid by containing approximately 550 mM/kg NaCl and varying amounts of dissolved Ca. The stock solutions had a natural Ca isotope composition and excess Ca relative to SO_4 to ensure that the majority of SO_4 was sequestered during anhydrite precipitation. Ca and SO_4 were added as the salts $CaCl_2$ and Na_2SO_4. Since no other sources of SO_4 were added, it is assumed that the mass of anhydrite does not change appreciably over the course of the experiments.

Importantly, these experiments utilized an isotope spike of enriched ^{43}Ca to track reaction progress over time. The enriched isotope spike overwhelms the natural isotopic composition and allows exchange between fluid and anhydrite to be tracked as a function of the fluid $\delta^{43}Ca$ values with increasing reaction time (Criss, 1999). Given that natural isotopic fractionation will be negligible in comparison to the spike, this method does not require prior knowledge of the equilibrium isotope fractionation factor (Johnson et al., 2004).

The ^{43}Ca spike solution had $^{43}Ca/^{42}Ca = 37.61$, a Ca concentration of 0.11 mmol/kg for experiment A and 0.35 mmol/kg for experiment B. The $^{43}Ca/^{42}Ca$ ratio of the experimental spike is much larger than the natural ratio, 0.21 (DePaolo, 2004) The spike solution was injected with a Teledyne ISCO syringe pump at the pressure-temperature conditions of the experiments. Each injection of anomalous ^{43}Ca was followed by injection of ~1–2 g of 550 mmol/kg NaCl fluid in order to ensure that all of the spike solution entered the gold cell and to prevent anhydrite precipitation in the capillary exit tube. The entire experimental system was cooled and disassembled after experiment A. Experiment C was initiated as an extension of experiment B by injecting a solution with 95 mmol/kg Ca and natural isotopic abundance to the contents of experiment B after the final sample of B. Upon termination of experiments A and C, anhydrite was filtered from solution within approximately 2 h from the start of cooling.

Unlike in the phase separation experiments, the ISCO syringe pump did not maintain constant pressure during the isotope exchange experiments. However, due to the small size of each sample (1–2 g) and the relatively large volume of spike injections (10–15 g), the overall system pressure did not drop below 45.0 MPa, well above the two-phase boundary at this temperature, 30.6 MPa (Bischoff and Pitzer, 1989). Upon addition of the ^{43}Ca spike, the autoclave and gold cell were rocked for 10 min to promote even distribution of the anomalous fluid. The furnace was not rocked during the remainder of the experiment.

2.3. Modern vent fluids

Fifty-one hydrothermal vent fluids from two different basalt-hosted systems (Juan de Fuca Ridge, East Pacific Rise 9-13°N) were collected with HOV Alvin as part of multidisciplinary research cruises over the past 20 years (Seyfried et al., 2003; Foustoukos and Seyfried, 2007a; Foustoukos et al., 2009; Pester et al., 2011, 2014). Fluids were collected using two types of titanium gas-tight isobaric samplers (Seewald et al., 2002; Wu et al., 2011), both of which minimize entrainment of bottom seawater during sampling. These two samplers show good reproducibility of vent fluid chemistry when used in the same vent location. Both samplers benefit from a thermocouple that is mounted along the side of the snorkel. ICL communication (Bradley

et al., 2001; Seewald et al., 2002; Wu et al., 2011) with the thermocouple readout and sampler inlet valve ensures that the measured fluid temperature coincides with the sampled fluid. On board ship, fluids for Ca isotope analysis were placed in acid-washed Teflon or low-density polyethylene bottles.

2.4. Analytical measurements

Elemental concentrations of experimental and field samples were determined in the Aqueous Geochemistry laboratory in the University of Minnesota Department of Earth Sciences. Inductively coupled plasma optical emission spectroscopy (ICP-OES) was used for cation analysis, while ion chromatography (IC) was used for anion determination. Uncertainty for the ICP-OES is 3% and 2% for IC (2σ). pH (25 °C, 1 atm) was measured using a Thermo-Ross electrode that was calibrated with pH 4, 7 and 10 buffers before each measurement. No calculations were performed to compensate for the liquid junction potentials that may occur when measuring pH of high salinity samples (Knauss et al., 1990).

Ca isotope compositions of all samples were measured on a Thermo-Fisher Neptune Plus multicollector-inductively coupled plasma mass spectrometer (MC-ICP-MS) at Princeton University. Samples for Ca isotope analyses were processed using an automated high-pressure IC system (Dionex ICS-5000+) and measured for $^{44}Ca/^{42}Ca$ and $^{44}Ca/^{43}Ca$ ratios following previously published methods (Fantle and Tipper, 2014; Blättler et al., 2015; Husson et al., 2015). All data are reported in delta notation relative to a known standard for Ca isotopes (Table 2) and measured $\delta^{44/42}Ca$ values were converted to $\delta^{44/40}Ca$ values assuming mass-dependent fractionation with a slope of 2.05 and no excess radiogenic ^{40}Ca (Fantle and Tipper, 2014). $\delta^{43}Ca$ values were calculated based on the reported $\delta^{44/43}Ca$ and $\delta^{44/40}Ca$ values. Although almost all of the Sr^{2+} is separated from Ca during ion chromatography, we corrected for occasional small Sr^{2+} isobaric interferences in the Ca measurements using measurements at $m/z = 43.5$ (doubly-charged $^{87}Sr^{2+}$). With the exception of samples with ^{43}Ca spikes, all measured Ca isotope compositions are plotted in three-isotope space ($\delta^{44/42}Ca$ vs. $\delta^{43/42}Ca$) to verify that the observed variability falls along the expected mass-dependent line (Fig. 1).

Long-term external reproducibility for our measurements is based on the difference between two known standards taken through the full chemical procedure (column chromatography and mass spectrometry) with each batch of samples. Our measured $\delta^{44/40}Ca$ value for SRM915b relative to modern seawater is $-1.18 \pm 0.08‰$ (1σ, $n = 9$), indistinguishable from published values determined by both MC-ICP-MS and TIMS (Fantle and Tipper, 2014). All Ca isotope samples are reported relative to modern seawater ($\delta^{44/42}Ca_{seawater} = 0.36 \pm 0.08‰$ (1σ, $n = 9$) and $\delta^{44/40}Ca_{seawater} = 0.02 \pm 0.11‰$ (1σ, $n = 9$)). $\delta^{44}Ca_{seawater} = +1.92‰$ on the SRM915a scale and $+0.98‰$ on the bulk silicate Earth (BSE) scale (Fantle and Tipper, 2014). Reported errors are equal to that of standard SRM 915b (for samples analyzed once) or 1 standard error of the mean

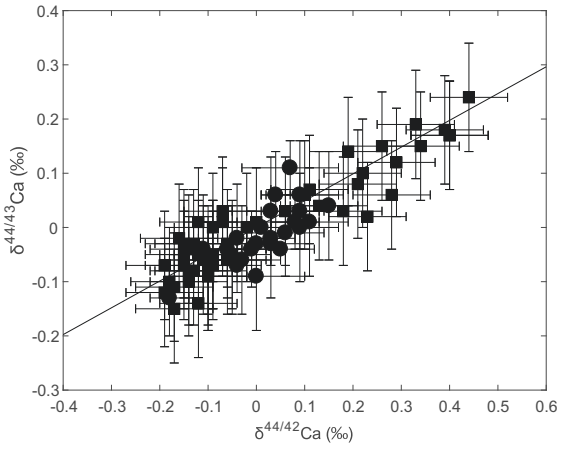

Fig. 1. $\delta^{44/43}Ca$ versus $\delta^{44/42}Ca$ for all samples with natural abundance Ca isotope composition. The natural abundance Ca isotope data from this study correlate well with the theoretical mass dependent fractionation line (slope ≈ 0.494). Circles represent experimental samples and squares represent natural vent fluids. Error bars are 2 SE for $\delta^{44/43}Ca$ and $\delta^{44/42}Ca$.

(SE) for samples with replicate analyses. For some samples with ^{43}Ca spikes the reproducibility of the $^{44}Ca/^{43}Ca$ ratios was significantly worse than unspiked samples. Although we cannot conclusively point to a cause, this added uncertainty in $^{44}Ca/^{43}Ca$ does not contribute significantly to the results presented here given the large signals observed in the ^{43}Ca spike experiments. In addition, two samples, B.1 and B.2, plot off the line, an artifact we attribute to contamination by a ^{43}Ca spiked sample during processing. However, since experiment B was spiked with anomalous $\delta^{43}Ca$ after sample B.2 small deviations in samples B.1 and B.2 do not change the calculated mass balance.

Imaging and chemical analysis of the product anhydrite from all experiments were performed with a Hitachi SU8230 scanning electron microscope (SEM) equipped with a Thermo System 7 EDS, housed in the Characterization Facility at the University of Minnesota. Images were taken with a 3.0 kV accelerating voltage, a probe current of 50 pA and a working distance of 8–8.5 mm. EDS spectra were acquired with a 15.0 kV accelerating voltage, probe current of 20nA and a working distance of 15 mm (Appendix).

2.5. Thermodynamic calculations

Aqueous speciation and activity calculations were performed using a thermodynamic database that accounts for the experimental temperature and pressure (410 °C, 50.0 MPa) of the isotope exchange experiments. The database was created using DBCreate (Kong et al., 2013), a software program that facilitates creation of thermodynamic databases at user defined pressure and temperature conditions. The initial thermodynamic data and included aqueous species are consistent with SUPCRT92 (Johnson et al., 1992). The Helgeson-Kirkam-Flowers equations of state, and subsequent revisions, are used to extrapolate

Table 2
Isotopic composition of phase separation experiments.

Sample	Reaction time (hours)	Pressure (MPa)	Phase	$\delta^{44/42}$ Ca	1 SE	$\delta^{44/43}$ Ca	1 SE	$\delta^{44/40}$ Ca	1 SE	N (replicates)
Experiment 1–420 °C										
Stock Solution				−0.11		−0.04		−1.10		1
1.3	–	37.5	1 phase	0.08	0.02	0.01	0.05	−0.73	0.03	2
1.4	19.75	32.5	Vapor	0.03	0.03	−0.02	0.01	−0.82	0.04	2
1.5	21.00	32.5	Liquid	0.09	0.02	0.03	0.02	−0.69	0.03	2
1.6	72.25	31.7	Liquid	0.01	0.02	0.00	0.01	−0.87		1
1.7	72.25	31.7	Vapor	−0.18		−0.13		−1.10		1
Product anhydrite				−0.29	0.01	−0.21	0.01	−1.42	0.03	2
Experiment 2–450 °C										
Stock solution				0.00	0.01	−0.03	0.01	−0.67	0.13	2
2.1	12.75	46.0	1-phase	0.04	0.03	0.06	0.08	−0.58	0.09	2
2.2	23.75	40.5	Vapor	−0.06	0.08	−0.04	0.07	−0.78	0.01	2
2.3	23.00	39.5	Vapor	0.03		−0.03		−0.83		1
2.4	25.75	38.5	Vapor	−0.04		−0.02		−0.69		1
2.5	28.00	37.5	Vapor	−0.03		−0.06		−0.68		1
2.6	24.00	40.5	Liquid	0.09		0.06		−0.71		1
2.7	24.00	39.5	Liquid	0.03		0.03		−0.78		1
2.8	22.50	38.5	Liquid	−0.04	0.05	−0.07	0.03	−0.74	0.06	2
2.9	23.25	37.5	Liquid	−0.01	0.03	−0.04	0.07	−0.68	0.09	2
Product anhydrite				−0.18		−0.22		−1.17		1

Ca isotopes expressed as,
$\delta^{X}Ca = [(R^{x/40}/R^{x/40}_{SW}) - 1] \times 1000$ (‰).
x = 43 or 44 and SW refers to the modern seawater standard.
Samples analyzed only once are assigned the error (1σ) of standard SRM915b in the same analytical session,
$\delta^{44/42} = 0.04$‰, $\delta^{44/43} = 0.05$‰, $\delta^{44/40} = 0.08$‰.

the necessary thermodynamic properties (Helgeson and Kirkham, 1974; Helgeson et al., 1981; Tanger and Helgeson, 1988) to experimental conditions and the extended Debye-Hückel equation is used to calculate activity coefficients of charged species. The standard state for pure minerals and pure water is unit activity, while the standard state of aqueous components is unit activity in a hypothetical one molal solution, referenced to infinite dilution. The modified database is compatible with Geochemist's Workbench (Bethke, 2008) and the measured concentrations of the dissolved components, Ca, Na, Cl, SO_4 and $pH_{25°C}$, serve as inputs to the appropriate mass action and charge balance equations.

3. RESULTS

3.1. Phase separation experiments

NaCl concentrations from phase separation experiments performed as part of this study agree well with predictions based on the numerical model of Driesner (2007) and Driesner and Heinrich (2007) and indicate equilibrium conditions for the NaCl-H_2O system (Fig. 2, Table 1). The agreement in NaCl concentrations also highlights the accuracy of the temperature and pressure control systems used in these experiments. Dissolved Ca and SO_4 concentrations follow a similar pattern to NaCl of enrichment in the liquid phase and depletion in the vapor phase relative to the single-phase fluid.

Prior to phase separation in experiment 1, the $\delta^{44}Ca$ composition of the single-phase fluid was −0.73‰ (Table 2). Upon phase separation, the $\delta^{44}Ca$ of the vapor phase decreased to −0.82 and −1.10‰, while the coexisting liquid varied between, −0.69 and −0.87‰. In experiment 2, the $\delta^{44}Ca$ composition of the single-phase solution was −0.58‰, the vapor ranged from −0.68 to −0.83‰, and the liquid varied from −0.68 to −0.78‰. In both experiments, the $\delta^{44}Ca$ signature of coexisting vapor and liquid pairs are the same, within error. The product anhydrite from the two experiments displayed $\delta^{44}Ca = -1.42 \pm 0.03$‰ (Exp. 1) and -1.17 ± 0.07‰ (Exp. 2).

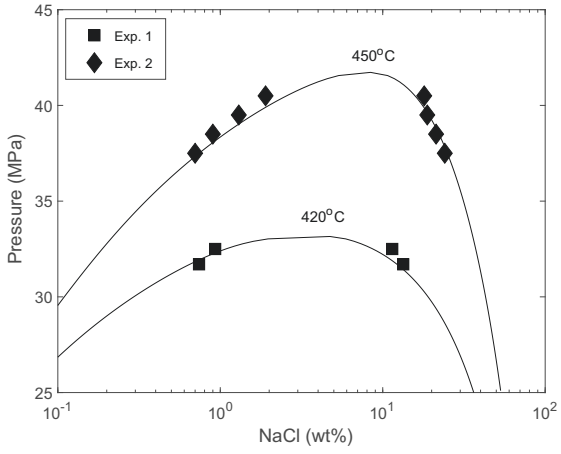

Fig. 2. NaCl composition of all samples taken during the phase separation experiments plotted against the predicted isotherms (solid lines) of Driesner (2007) and Driesner and Heinrich (2007). NaCl concentrations are the average of measured Na^+ and Cl^-. The good agreement between experimental data and model isotherms suggest the bulk matrix achieved chemical equilibrium and highlights the accuracy of the experimental pressure-temperature system.

The distribution of chemical species that is responsible for vapor-liquid isotopic fractionation has been shown to reach equilibrium within minutes to hours during phase separation at temperatures and pressures consistent with the present investigation (Bischoff et al., 1986; Pokrovski et al., 2005). Therefore, in keeping with previous studies of vapor-liquid isotopic fractionation (Liebscher et al., 2005, 2006; Rempel et al., 2012), samples taken during the phase separation experiments were allowed to react for approximately 24 h at constant pressure and temperature to ensure vapor-liquid isotopic equilibrium (Table 2). Isotopic exchange rates in heterogeneous systems (mineral-fluid) are considerably slower, even at hydrothermal temperatures and pressures, than the homogeneous counterpart (fluid-fluid) (Cole and Chakraborty, 2001). Thus, it is possible that the anhydrite did not precipitate from solution in isotopic equilibrium with the fluid (Johnson et al., 2004; DePaolo, 2011). This will not change the magnitude of vapor-liquid isotope fractionation, which is ultimately controlled by the rapid distribution of aqueous species and their associated coordination chemistry. It is, however, important to determine the rate of Ca fluid-mineral exchange, which can best be accomplished for a single-phase fluid coexisting with anhydrite at a temperature consistent with the phase separation experiments.

3.2. Isotope exchange experiments

In order to isolate the effects of isotopic mineral-fluid exchange from those associated with net precipitation or dissolution of anhydrite, experiments were run to chemical equilibrium prior to the injection of the ^{43}Ca spike. Equilibrium was assessed by comparison of the calculated $Ca^{2+}_{(aq)}$ and $SO^{2-}_{4(aq)}$ activities with the theoretical fluid-anhydrite phase boundary (Fig. 3). Predicted and measured Ca concentrations are within 15% for all three experiments, and the results from experiments A and C plot close to the phase boundary, suggesting chemical equilibrium (i.e. anhydrite saturation) was achieved. For experiment B (Table 3), the reported SO_4 concentration is below the analytical detection limit and is therefore replaced with the detection limit of 40 μmol/kg. Given the good agreement in predicted and measured Ca, experiment B also reached chemical equilibrium. That the fluid chemistry for this experiment suggests anhydrite under saturation reflects the difficulty of measuring such low SO_4 concentrations. pH (25 °C, 1 atm) varied between 5.12 and 5.93 and shows no apparent pattern with time. Ca and SO_4 concentrations decreased after an injection as the result of mixing between fluids with slightly different Ca and SO_4 compositions and the 550 mM/kg NaCl solution used to flush the reactor capillary tubing. Speciation calculations confirm that post-injection samples were also anhydrite saturated.

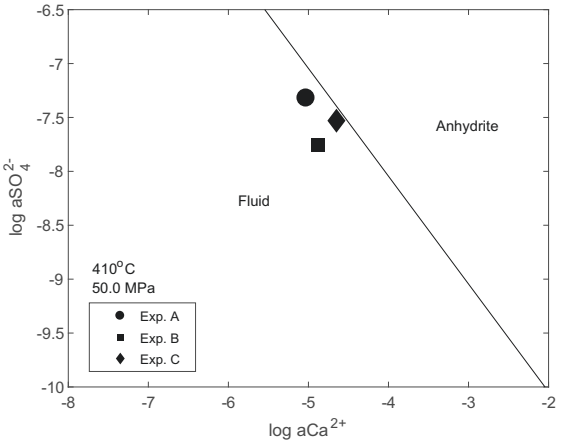

Fig. 3. Fluid-anhydrite phase diagram at the pressure-temperature conditions of the isotope exchange experiments. All three experiments plot near the phase boundary suggesting fluid-anhydrite chemical equilibrium was achieved.

Fluid samples from all experiments containing isotopic spikes exhibit large δ^{43}Ca values (>78‰, Table 3) and initial, $t = 0$, δ^{43}Ca compositions are calculated by linear regression of subsequent samples (see Appendix). The δ^{43}Ca of the system (fluid + anhydrite) is calculated by mass balance using the δ^{43}Ca of the stock solution as the starting value and accounting for the injection of anomalous δ^{43}Ca and mass loss associated with sampling. As expected, δ^{43}Ca of the solution decreased with reaction time as the ^{43}Ca spike in the fluid exchanged with the natural abundance ^{43}Ca in the anhydrite. The decline in fluid δ^{43}Ca for experiments A, B and C are 52.7‰, 42.2‰ and 3.51‰, respectively. Experiment C displays a smaller range of δ^{43}Ca because the anhydrite had elevated δ^{43}Ca remaining from experiment B and the fluid δ^{43}Ca composition was lowered significantly by injection of natural abundance Ca (see experimental procedures). The uncertainty in δ^{43}Ca and small changes in these values between samples makes it difficult to unambiguously resolve the rate of Ca mass transfer in experiment C.

The dissolution of anhydrite during quench, as described below, makes the recovered anhydrite an unreliable constraint on the Ca isotopic composition of this phase and coexisting fluid at experimental conditions. Nevertheless, $\Delta^{44}Ca_{anh\text{-}fluid}$ can be calculated prior to injection of the ^{43}Ca spike solution. $\Delta^{44}Ca_{anh\text{-}fluid}$ for experiments A and B are approximately −0.41‰ and −0.94‰, respectively. The large difference between these values and the short amount of reaction time (<96 h) indicate these isotopic fractionations are not indicative of equilibrium. Experiment C is not included as ^{44}Ca was altered by the presence of the spike in all samples in this experiment.

The extent of isotopic mixing between fluid and anhydrite, F, can be quantified as follows (Criss et al., 1987)

$$F = \frac{\delta_t^{43}Ca - \delta_0^{43}Ca}{\delta_{\Sigma Ca}^{43}Ca - \delta_0^{43}Ca} \quad (1)$$

where the subscripts 0 and t refer to the initial fluid composition (time of spike addition) and at any subsequent sampling time, respectively. The subscript ΣCa refers to the bulk composition (fluid and mineral) of the system. Given that the anhydrite-fluid Ca isotope fractionation is expected to be small at experimental conditions, a highly enriched ^{43}Ca spike justifies the use of $\delta_{\Sigma Ca}^{43}$Ca in place of the equilibrium fluid δ^{43}Ca in Eq. (1) (Johnson et al., 2004; Handler et al., 2014).

F is a parameter that expresses approach to equilibrium for a specific chemical system at well-defined pressure and temperature conditions and can be used to determine the order of a given reaction. Previous studies of isotope exchange in both homogeneous and heterogeneous systems have been often described with first order reaction schemes (Cole et al., 1983; Johnson et al., 2004; Frierdich et al., 2014), although this is not always the case (Graham, 1981; Johnson et al., 2002). In keeping with previous studies that investigate isotopic exchange between NaCl-fluids and sulfate minerals (Kusakabe and Robinson, 1977; Chiba et al., 1981), we describe the relationship between F and time using a first order reaction

$$\ln(1 - F) = -kt \quad (2)$$

The rate constant, k, is calculated as the slope of a least squares fit to the data. The R^2 for the least squares fit was greater than 0.9 for all three experiments. For experiments A, B, and C, the rate constants calculated with Eq. (2) have units of hr^{-1} and are 6.9×10^{-4} ($\pm 3.0 \times 10^{-5}$), 1.2×10^{-3} ($\pm 1.6 \times 10^{-4}$), and 1.0×10^{-3} ($\pm 1.0 \times 10^{-4}$), respectively (Fig. 4). Eq. (2) can be modified in order to account for the dissolved Ca concentration

$$\ln(1 - F) = -k[Ca]t \quad (3)$$

While previous studies (e.g. Criss et al., 1987) have included terms to account for moles of reactive isotope in each phase, we use a concentration term since it is the moles per gram (or mL) of water that ultimately determines the frequency of molecular collision and thus reaction rates (Lasaga, 1981a). The three rate constants ($kg_{sol'n}$ $mmol^{-1}$ hr^{-1}) calculated using Eq. (3) are 5.8×10^{-5} ($\pm 2.5 \times 10^{-6}$), 5.3×10^{-5} ($\pm 6.9 \times 10^{-6}$), and 2.3×10^{-5} ($\pm 2.4 \times 10^{-6}$), for experiments A (12 mM/kg Ca), B (23 mM/kg Ca) and C (45 mM/kg Ca), respectively. The values from experiments A and B are averaged to give an overall rate constant of 5.6×10^{-5}. Using this average rate constant and the dissolved concentrations of experiments A and B in Eq. (3), 142 and 74 days, respectively, are required to achieve 90% anhydrite-fluid isotope exchange. The rate constant from experiment C is not included in the average, as it would unrealistically skew the result, since the value of F did not increase between experiments B and C after the same amount of reaction time (Table 3). It is important to remember that experiment C began as an extension of experiment B. Given that the anhydrite surface area evolved differently in experiments A and B then it did in C, as discussed below, we do not directly compare the results of experiment C with those of A and B.

In many mineral-fluid isotopic and chemical exchange reactions, the surface area of the mineral contributes to the overall rate of exchange (Cole and Chakraborty, 2001; Brantley et al., 2008 and references therein). SEM

Table 3
Chemical and isotopic composition of fluid and anhydrite in isotope exchange experiments.

Sample	Time after injection of spike (hours)	Ca (mM)	SO_4 (μM)	pH_{25C}	$\delta^{44/42}$ Ca	1 SE	$\delta^{44/43}$ Ca	1 SE	$\delta^{44/40}$ Ca	1 SE	$\delta^{43/40}$ Ca	1 SE	N	F (%)*
Experiment A														
Stock solution		44.0	22,600	5.63	−0.11		−0.04		−1.11				1	
A.1		19.6	199	3.23	0.11		0.01		−0.57				1	
A.2		19.3	96	5.35	0.15		0.04		−0.57				1	
A.3		18.8	69	5.12	0.09		0.00		−0.69				1	
A.4		18.6	64	5.55	0.05	0.01	−0.04	0.01	−0.56	0.02			2	
Spike	0	0.11	BDL											
A.5	0.75	12.5	57	5.69	4.14		−285.87		7.66		411.23			0.09
A.6	3.5	12.8	53	5.93	3.94	0.08	−278.26	0.25	7.27	0.17	395.61	0.54	2	0.33
A.7	7	12.5	51	5.70	3.83	0.02	−272.18	0.79	7.09	0.01	383.71	1.50	2	0.77
A.8	20	12.5	48	5.46	3.94		−275.23		7.58		390.21		1	2.24
A.9	44.25	12.4	47	5.38	3.90		−271.90		7.17		383.29		1	4.64
A.10	92.25	12.3	45	5.35	3.72		−267.04		6.80		373.61		1	7.87
A.11	169.75	12.0	BDL	5.35	3.56	0.15	−260.28	0.22	6.65	0.14	360.85	0.45	2	12.04
A.12	282.75	11.8	BDL	5.44	3.46	0.06	−250.52	0.48	6.43	0.03	342.84	0.86	2	17.82
A-Anhydrite					−0.08		−13.57		−0.97		12.77		1	
Experiment B														
Stock solution		46.9	18,500	4.82	0.00		−0.09		−0.89				1	
B.1		27.5	BDL	5.03	0.16		−0.39		−0.51				1	
B.2		27.1	BDL	5.54	0.21		−0.48		−0.40				1	
Spike	0.0	0.35	BDL											
B.3	0.9	23.5	BDL	5.73	3.68		−256.97		6.72		354.88			0.37
B.4	6.3	23.9	BDL	5.86	3.20	0.02	−232.72	0.10	5.76	0.06	310.81	0.19	2	2.22
B.5	22.3	23.6	BDL	5.72	3.06		−227.39		5.45		301.37		1	8.65
B.6	32.7	23.6	BDL	5.50	3.04		−224.58		5.50		296.72		1	11.51
B.7	48.5	23.3	BDL	5.67	3.00	0.06	−224.31	0.10	5.39	0.08	296.12	0.20	2	11.55
B.8	74.3	23.0	57	5.88	3.09	0.10	−221.40	0.70	5.52	0.19	291.45	1.19	2	14.15
B.9	243.3	22.8	53	5.60	2.77		−207.75		4.88		268.39		1	27.81
Experiment C														
NIS	0	94.9	BDL	5.58	0.06	0.08	−0.01	0.01	−0.72	0.04			2	
C.1	1.25	46.3	55	5.50	0.89		−72.90		1.03		79.74		1	0.41
C.2	5.25	45.9	56	5.54	0.80		−74.63		0.82		81.53		1	8.53
C.3	20.50	45.4	52	5.66	0.90	0.07	−74.67	0.51	1.18	0.08	81.97	0.43	2	4.89
C.4	29.75	45.1	56	5.61	0.93		−74.16		1.10		81.29		1	9.71
C.5	46.75	44.5	55	5.61	0.81		−74.34		0.92		81.30		1	9.20
C.6	56.75	44.3	51	5.89	0.87		−73.50		0.96		80.37		1	15.09
C.7	72.00	44.0	50	5.72	0.84		−73.65		0.92		80.50		1	13.65
C.8	96.25	47.9	52	5.67	0.85		−73.40		0.93		80.22		1	14.76
C.9	242.25	45.8	BDL	5.79	0.80		−71.63		0.80		78.02		1	27.01
C-Anhydrite					0.43		−51.71		0.08		54.61		1	

mM = mmol/kg of solution, uM = μmol/kg of solution.
Samples analyzed only once are assigned the 1 SE of standard 915b in the same analytical session, $\delta^{44/42} = 0.04‰$, $\delta^{44/43} = 0.05‰$, $\delta^{44/40} = 0.08‰$.
NIS = Natural injection solution, solution of natural δ^{43}Ca injected to reset bulk elemental and isotopic Ca.
1 SE for $\delta^{43/40}$ Ca for samples analyzed once is 0.67‰, the average of the measured errors.
BDL = below detection limit.
* F (%) calculated with adjusted δ^{43}Ca.

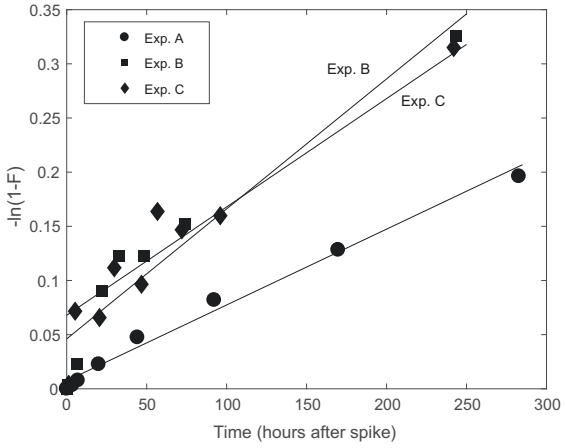

Fig. 4. First order kinetic representation (Eq. (2)) of data from the isotope exchange experiments. The solid lines represent linear regressions through the data, the slope of which is equal to the rate constant for each experiment. See section 3.2 for discussion.

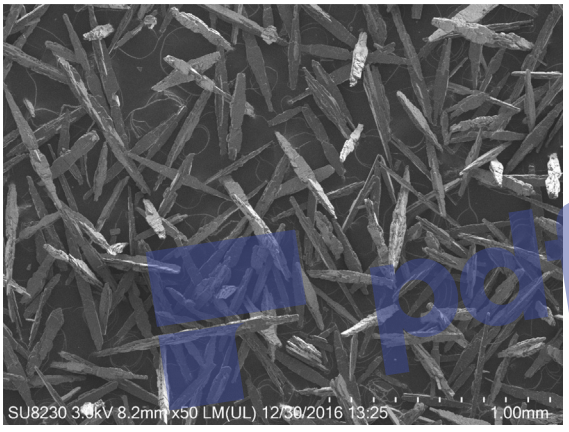

Fig. 5. SEM image showing representative anhydrite crystals from isotope exchange experiment A. The product anhydrite from both phase separation (not shown) and isotope exchange experiments are similar in size and morphology and therefore surface area is not explicitly accounted for in the rate law. The crystals show signs of dissolution and post experiment fracturing and therefore the original surface area is estimated as a right rectangular prism. See section 3.2 for details.

images of anhydrite from the present study demonstrate that the product anhydrite from the phase separation and isotope exchange experiments has acicular morphology and also shows clear evidence of dissolution (Fig. 5). The isotope exchange experiments were designed specifically to measure in-situ fluid chemistry and dissolution was predictable given the relatively long amount of time (2 h) needed to cool the steel pressure vessel and gold reaction cell. About half as much anhydrite was recovered as expected, based on mass balance calculations of the first several samples. This indicates that the observed defects in the crystal structure almost certainly occurred during cooling. Crystals that appear to be completely intact measure between 1 and 1.5 mm in length, while smaller crystals present in the image are interpreted to have broken mechanically during post experiment processing. Given that anhydrite in the experiments (isotope exchange (A and B) and phase separation) formed by heating of Ca and SO_4 rich fluid, the evolution of surface area over the course of the experiments (heat up and constant temperature recrystallization) is assumed to be equal. That the Ca normalized rate constants for experiments A and B, $5.8 \times 10^{-5} \pm 2.5 \times 10^{-6}$ and $5.3 \times 10^{-5} \pm 6.9 \times 10^{-6}$ ($kg_{sol'n}$ $mmol^{-1}$ hr^{-1}), are the same within error also suggests that differences in surface area did not substantially alter the rate of exchange.

In lieu of direct measurements, the surface area of the pristine anhydrite crystals in all experiments can be estimated geometrically as a right rectangular prism. Based on the SEM images, the dimensions chosen are $1250 \times 100 \times 60$ μm, yielding a surface area of 4.12×10^{-3} cm^2 and a volume of 7.5×10^{-6} cm^3. The density of anhydrite is 2.98 g/cm^3 (Palache et al., 1951), which together with our calculated volume and surface area gives a specific surface area of 1.84×10^{-2} m^2 g^{-1}.

As demonstrated by Chiba et al. (1981), a decrease in the solution pH increases the rate of O isotope exchange between fluid and anhydrite. These authors hypothesize that the activity of H^+ plays a fundamental, but uncertain, role in exchange kinetics. Thermodynamic modeling using measured element concentrations indicate that at conditions of our experiments the in-situ pH is 5.95, 5.83 and 5.78 for experiments A, B and C, respectively. Thus, differences in pH between experiments are insufficient to alter the rates of exchange in this study.

3.3. Vent fluid Ca isotopes

The Ca isotope compositions ($\delta^{44}Ca$) of hydrothermal vent fluids ($n = 51$) issuing from East Pacific Rise (EPR)

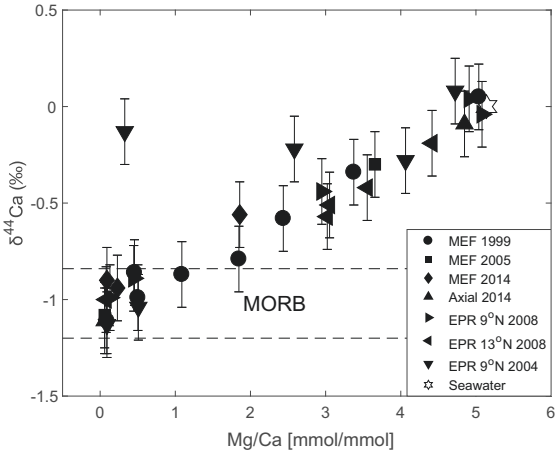

Fig. 6. $\delta^{44}Ca$ values for vent fluids from four different hydrothermal sites and the modern seawater standard plotted against the respective Mg/Ca ratios. End member fluids (Mg/Ca approaching 0) show $\delta^{44}Ca$ values that agree with the MORB value, -1.02 ± 0.18‰ (SW). Linear regression of all data yields $\delta^{44}Ca = -1.04 \pm 0.03$‰ (SW). For each vent site, samples with Mg/Ca < 0.2 were averaged to improve the clarity of this figure. MEF = Main Endeavor Field, Juan de Fuca Ridge, Axial = Axial Caldera, Juan de Fuca Ridge, EPR = East Pacific Rise.

9–13°N and Juan de Fuca Ridge (JdFR) vary between 0 and −1.2‰ (SW) and exhibit a clear linear correlation with the dissolved Mg/Ca ratios (Fig. 6). The extrapolated end-member (Mg/Ca = 0) δ^{44}Ca for the entire data set is −1.04‰ and end-member δ^{44}Ca for each vent site vary from −0.98 to −1.12‰ (Table 4). Complete vent chemistry for MEF (1999 and 2005), EPR 9°N (2004 and 2008) and EPR 13°N (2008) have been published previously (Seyfried et al., 2003; Foustoukos and Seyfried, 2007a; Foustoukos et al., 2009; Pester et al., 2011, and Pester et al., 2014).

4. DISCUSSION

4.1. Anhydrite-fluid Ca isotope exchange

In order for Ca isotopes to be used effectively as geochemical and environmental proxies, the mechanisms that produce mineral-fluid fractionation must be well understood. Ca isotope fractionations between minerals, primarily calcite, and aqueous solutions have been interpreted to represent both kinetic (Tang et al., 2008; DePaolo, 2011; Brown et al., 2013) and equilibrium (Bullen et al., 2003; Marriott et al., 2004) fractionation. Inherent to the discussion regarding kinetic or equilibrium fractionation is the mechanism and rate at which Ca isotopes exchange between coexisting reservoirs. Such data are limited for the Ca system at ambient and elevated temperatures, but necessary to inform our interpretation of observed experimental and natural Ca isotope systematics.

At the elevated temperature (410 °C) of the isotope exchange experiments, both recrystallization and diffusion could potentially control isotopic mixing between fluid and anhydrite. Comparison of the rate constants (Eq. (2)) regressed from this study with that of another study that investigated fluid-anhydrite O exchange at a range of hydrothermal temperatures shows good agreement characterized by largely similar temperature dependence (Fig. 7, Chiba et al., 1981). Below 200 °C diffusion is likely too slow to control exchange rates (Chacko et al., 2001; Johnson et al., 2004). Therefore the linear trend is important in that it demonstrates a single exchange mechanism, recrystallization (Chiba et al., 1981), dominates across the entire temperature range (100–550 °C) investigated. The range of activation energies calculated by Chiba et al. (1981), 42–46 kJ/mol, also suggests recrystallization as the dominant mechanism of exchange (Lasaga, 1981a). Experiments in which diffusion is the dominant exchange mechanism generally have activation energies between 84 and 125 kJ/mol (Lasaga, 1981b).

It is noteworthy that the rate of recrystallization in the isotope exchange experiments varies with different dissolved Ca concentrations (Fig. 8). Previous experiments have purposefully changed mineral solubility by altering the NaCl (or other salt) content in order to investigate the effect on oxygen isotope exchange (Chai, 1975; Cole et al., 1992; Cole, 1992). In these studies, an increase in mineral solubility dramatically increased the rate of oxygen isotope exchange between fluid and either granite or calcite. Anhydrite solubility in our experiments is extremely low at 410 °C owing to the well-known retrograde solubility. The presence of excess Ca in the fluid also prevents significant dissolved SO_4 from accumulating. The low solubility notwithstanding, our results suggest that changes in the concentration of the dissolved components can produce measurable effects on isotope exchange rates, even in systems at chemical equilibrium. This is in keeping with experiments performed in both the S and O isotope systems (Kiyosu, 1973; Ohmoto and Lasaga, 1982; Cole et al., 1983; Syverson et al., 2015).

As an example of the utility of isotopic exchange rate data, the extent of Ca isotopic mixing between anhydrite and fluids in the phase separation experiments is assessed. The phase separation experiments reacted for approximately 24 h at each individual pressure and temperature and experiments 1 and 2 cumulatively lasted 185 and 207 h, respectively (Table 2). Calculations indicate that after 24 h, roughly 5% of the Ca in the anhydrite exchanged with the fluid phase (see Appendix). After 185 and 207 h, between 10 and 14% Ca in the anhydrite exchanged. These are minimum values given that they were calculated at 410 °C and the phase separation experiments took place at 420 and 450 °C. Additionally, the phase separation experiments involved fluid:anhydrite Ca mole ratios of approximately 2 and 3. These ratios are higher than in the isotope exchange experiments and would also increase the rate of anhydrite-fluid Ca isotope exchange (Handler et al., 2014). Altering the fluid Ca concentration in experiment B to impose a fluid:anhydrite Ca ratio of 3 increases the percent of anhydrite Ca exchanged by the same factor, so that after 185 or 207 h there is approximately 45% exchange. While difficult to calculate the exact amount of exchange that occurred in the phase separation experiments, the lack of change in the isotopic composition of the vapor and liquid, particularly in experiment 2 (450 °C), suggests that significant variation would be unlikely if the experiments had reacted further.

4.2. Ca isotope systematics in mid-ocean ridge hydrothermal systems

Previous studies have produced contrasting interpretations of Ca isotope fractionation in mid-ocean ridge hydrothermal systems. Zhu and Macdougall (1998) suggest that fractionation is negligible due to the high temperatures involved. Amini et al. (2008) argue that the difference between end member hydrothermal fluid δ^{44}Ca and host rock δ^{44}Ca at the Logatchev vent field results from Ca fractionation during anhydrite precipitation. Phase separation produces vapors that are enriched in the heavy isotopes of Fe, Cl, B and H relative to the source fluid (Berndt et al., 1996; Liebscher et al., 2005, 2006; Syverson et al., 2014). A similar pattern in the Ca system could be another mechanism by which end member vent fluids display heavier δ^{44}Ca relative to that of the host rock.

End-member vent fluids taken from EPR 9°50′N and JdFR show δ^{44}Ca that do not vary substantially with total dissolved Cl concentration. As an example, the end-member δ^{44}Ca for Axial (JdFR, 2014) is −1.12‰ and Cl

Table 4
Chemical and isotopic composition of natural vent fluids.

	Sample	Mg (mM)	Ca (mM)	Mg/Ca	Cl (mM)	$\delta^{44/40}$Ca± 0.08‰ (1 SE)	$\delta^{44/42}$Ca± 0.04‰ (1 SE)	$\delta^{44/43}$Ca± 0.05‰ (1 SE)
MEF, 1999								
Hulk	BGT3478	2.8	32.5	0.1	447.0	−1.11	−0.18	−0.10
Dante	M3470A	13.3	26.5	0.5	446.0	−0.99	−0.10	−0.06
Bastille	BGT3470	5.8	12.7	0.5	239.0	−0.86	−0.05	−0.06
Bastille	M3470D	29.0	11.9	2.4	398.0	−0.58	0.21	0.08
Cantilever	BGT3474	2.4	1.3	1.8	54.0	−0.79	0.00	0.01
Cantilever	M3474A	8.1	2.4	3.4	109.0	−0.34	0.22	0.10
Sully	M3474B	2.5	2.3	1.1	62.0	−0.87	−0.05	−0.05
Sully	BGT3480	52.9	10.5	5.0	534.0	0.05	0.40	0.17
End member						−1.10		
MEF, 2005								
Dudley	M4132-23	2.5	35.5	0.1		−0.99	−0.10	−0.08
Puffer	IGT4134-5	1.1	28.7	0.04	459.0	−1.13	−0.17	−0.15
Sully	IGT4139-2	1.5	27.0	0.1	459.0	−1.00	−0.12	−0.14
Bastille	IGT4139-4	1.3	29.2	0.0	463.0	−1.10	−0.15	−0.07
Smoke and Mirrors (flange)	IGT4148-5	1.9	34.6	0.1	489.0	−1.03	−0.10	−0.09
Easter Island	IGT4142-4	48.2	13.2	3.7	540.0	−0.30	0.23	0.02
Easter Island	IGT4142-5	3.2	28.8	0.1	494.0	−1.18	−0.19	−0.07
Mothra (Hot Harold)	M4140-11	4.3	49.6	0.1		−1.10	−0.14	−0.10
Mothra (Faulty Towers)	CGT4143	2.0	50.7	0.0		−1.07	−0.13	−0.03
End member						−1.09		
MEF, 2014								
Lobo	4743D	1.6	40.0	0.0	540.0	−0.99	−0.06	−0.03
Bastille	4743C	5.6	24.6	0.2	456.0	−0.94	−0.07	0.03
Dante	4744 6-2	2.2	37.8	0.1	525.0	−0.83	−0.02	0.00
TP	4743E	2.1	38.4	0.1	522.0	−1.09	−0.13	−0.08
Sully (flange)	4743 6-4	29.4	15.8	1.9	508.0	−0.56	0.10	0.06
Lobo	4744 6-1	3.3	39.1	0.1	545.0	−1.03	−0.12	0.01
Puffer	4743 6-5	4.5	23.4	0.2	445.0	−0.89	−0.06	−0.06
End member						−0.98		
Axial, 2014								
Mushroom	4739E	2.9	49.9	0.1	706.0	−1.12	−0.16	−0.02
Inferno	4739D	2.0	49.4	0.0	706.0	−1.08	−0.14	−0.04
Hell	4739C	2.7	37.6	0.1	577.0	−1.11	−0.17	−0.11
Phoenix	4739B	2.4	38.2	0.1	581.0	−1.18	−0.15	−0.05
Gollom	4741B	50.8	10.5	4.8	569.0	−0.09	0.34	0.15
Hell	4741C	2.1	36.8	0.1	577.0	−1.19	−0.15	−0.03
Inferno	4741D	5.1	46.4	0.1	699.0	−1.05	−0.09	−0.05
Phoenix	4741E	2.0	39.2	0.1	584.0	−1.02	−0.10	−0.09
End member						−1.12		

(*continued on next page*)

Table 4 (*continued*)

	Sample	Mg (mM)	Ca (mM)	Mg/Ca	Cl (mM)	$\delta^{44/40}$Ca± 0.08‰ (1 SE)	$\delta^{44/42}$Ca± 0.04‰ (1 SE)	$\delta^{44/43}$Ca± 0.05‰ (1 SE)
EPR 9°50′N, 2008								
Bio 9	B9-4386-IGT6	1.9	13.9	0.1	313.0	−0.96	−0.07	0.01
Crab Spa	CS-4394-IGT6	49.3	10.1	4.9	520.0	0.04	0.39	0.18
Tica	TC-4388-IGT5	29.3	9.9	2.9	366.0	−0.44	0.18	0.03
P vent	P-4393-IGT5	2.0	17.3	0.1	387.0	−1.01	−0.09	−0.07
Ty/Io	TI-4393-IGT6	2.6	5.9	0.4	165.0	−0.89	0.06	0.03
Ty/Io	TI-4397-IGT5	51.0	10.0	5.1	532.0	−0.04	0.40	0.17
End member						−1.00		
EPR 13°N, 2008								
Actinoir	AC-4391-MW	47.3	10.7	4.4	528.0	−0.19	0.28	0.06
Dorian	DO-4391-MG	39.1	12.9	3.0	519.0	−0.57	0.11	0.07
Dorian	DO-4392-IGT5	2.3	21.2	0.1	466.0	−0.94	−0.09	−0.05
Ph	Ph-4392-IGT6	41.8	11.8	3.6	525.0	−0.42	0.19	0.14
Grand Bonum	GB-4389-IGT5	2.2	44.2	0.0	642.0	−1.06	−0.09	0.00
Jumeaux	JX-4392-MG	34.9	11.4	3.1	473.0	−0.51	0.13	0.04
End member						−1.03		
EPR 9°50′N, 2004								
Bio9	IGT-3961-1	1.5	12.7	0.1	328.0	−1.15	−0.19	−0.12
Bio9	M-3961-16	30.7	11.9	2.6	454.0	−0.22	0.29	0.12
P Vent	IGT-3964-4	1.3	22.0	0.1	546.0	−1.11	−0.14	−0.08
Tica Hi-T	M-3964-16	46.2	11.4	4.1		−0.28	0.26	0.15
Tica-Lo-T	IGT-3961-3	51.9	11.0	4.7		0.08	0.44	0.24
Q Vent	M-3972-15	15.3	30.0	0.5	577.0	−1.04	−0.11	−0.06
Bio9′	M-3969-16	3.5	10.6	0.3	292.0	−0.13	0.33	0.19
End member						−1.13		

mM = mmol/kg solution.
MEF = Main Endeavour Field, Juan de Fuca Ridge.
Axial = Axial Caldera, Juan de Fuca Ridge.
EPR = East Pacific Rise.

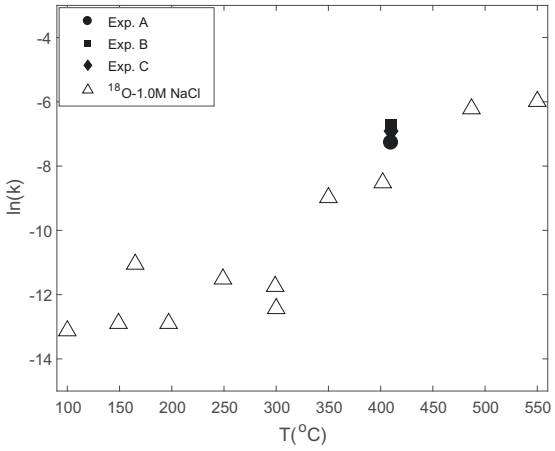

Fig. 7. Comparison of rate constants calculated with Eq. (2) for Ca (solid markers) and O (open markers, Chiba et al., 1981) anhydrite-fluid isotope exchange. The linear trend across the entire temperature range suggests a common exchange mechanism in all experiments. The range of activation energies, 42–46 kJ/mol, from the O experiments is indicative of recrystallization.

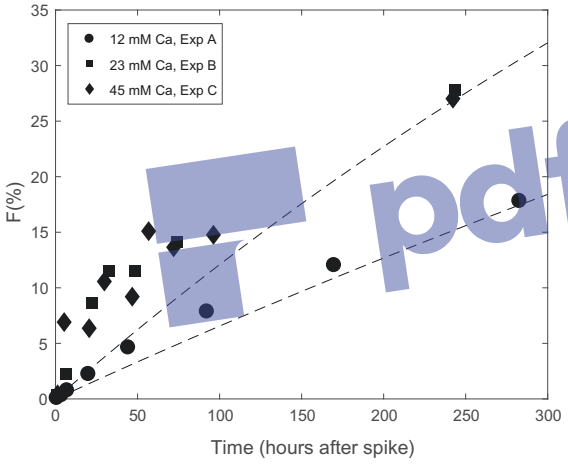

Fig. 8. F (Eq. (1)) as a function of time for the isotope exchange experiments. Symbols show the data points from the three experiments, while the dashed lines represent Eq. (3), calculated with the average rate constant (5.6×10^{-5} mmol^{-1} kg hr^{-1}), and the Ca concentration from experiments A and B. The overall rate of fluid-anhydrite Ca isotope exchange increases with increasing total dissolved Ca between experiments A and B.

concentrations from these vents are always greater than seawater. In contrast, vents sampled at EPR 9°50′N (2008) have less than seawater chlorinity and the end-member $\delta^{44}Ca = -1.00‰$ (Table 4). The natural vent samples coincide with our experimental results that indicate significant Ca isotope fractionation does not occur between vapor-liquid pairs (Fig. 9) within the pressure and temperature ranges investigated (31.0–37.5 MPa, 420 °C and 36.0–46.0 MPa, 450 °C). These conditions were chosen because similar conditions prevail for seafloor vent systems during steady state intervals between magmatic activity (Fontaine et al., 2009; Pester et al., 2014).

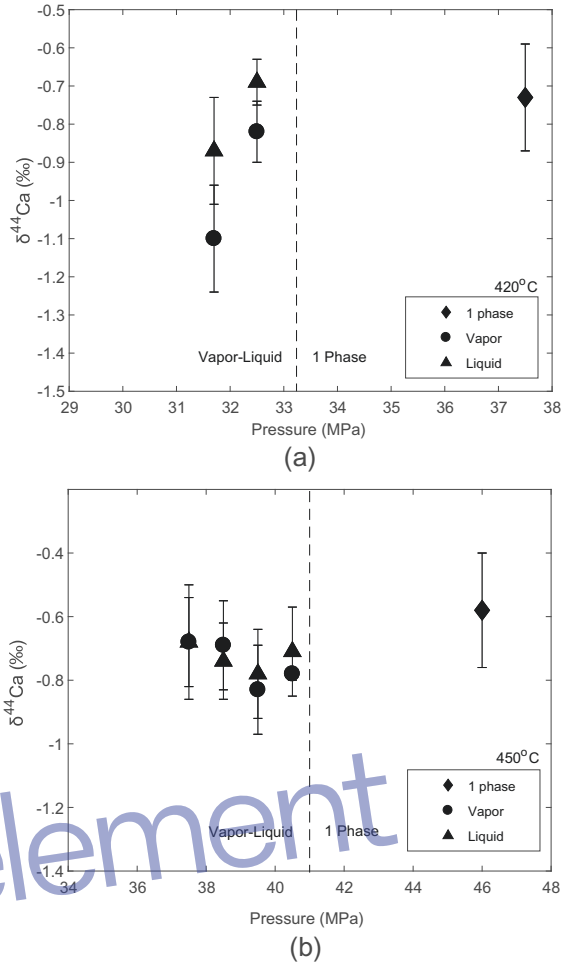

Fig. 9. $\delta^{44}Ca$ values as a function of pressure for phase separation experiments at 420 °C (a) and 450 °C (b). Within analytical error, there is no Ca isotope fractionation between vapor and liquid within the pressure-temperature ranges investigated. The chosen P-T conditions are representative of many fast-spreading hydrothermal systems during steady state. The lack of vapor-liquid fractionation is consistent with natural vent fluids that record MORB $\delta^{44}Ca$, regardless of dissolved Cl concentration.

A large dataset now exits indicating that the $\delta^{44}Ca$ composition of MORB is $-1.02 \pm 0.18‰$ (SW) (Wombacher et al., 2009; Amini et al., 2009; Schiller et al., 2012; Colla et al., 2013; Valdes et al., 2014; Lehn and Jacobson, 2015; Feng et al., 2017). The $\delta^{44}Ca$ composition of end-member vent fluid samples from the present study all lie within the MORB field (Fig. 6), as do end-member fluids from the Logatchev hydrothermal field, $-0.95 \pm 0.07‰$ (SW) (Amini et al., 2008), and 17° to 19°S on the East Pacific Rise, $-1.00 \pm 0.05‰$ and $-1.11 \pm 0.05‰$ (SW) (Schmitt et al., 2003). That mid-ocean ridge vent fluids record MORB $\delta^{44}Ca$ substantiates previous work (Zhu and Macdougall, 1998) that indicates that the primary effect of modern MOR hydrothermal systems is to trap seawater Ca and release mantle Ca to the ocean.

Isotopic and chemical measurements from MOR hydrothermal systems indicate that the hydrothermal fluid interacts with fresh basalt. Field and experimental studies

have shown that the constancy and similarity of Li isotope compositions from MOR vent fluids along the EPR, JdFR, and Mid-Atlantic Ridge (MAR) can best be explained by alteration of fresh basalt (Chan et al., 1992; Seyfried et al., 1998; Foustoukos et al., 2004). Reaction between low-temperature seawater and basalt results in altered basalt that is enriched in ^{7}Li relative to the fresh rock (Chan et al., 1992). This isotopic fractionation is useful in that it creates distinct Li isotope compositions between altered and unaltered basalt that can be used to assess sources of vent fluid Li. Fluids venting at EPR, JdFR and MAR record Li isotopic signatures consistent with alteration of fresh basalt; there is no evidence for interaction of fluid with weathered basalt based on Li isotope compositions, regardless of the dissolved Cs/Rb ratio (Chan et al., 1993; Foustoukos et al., 2004). Elevated vent fluid Cs/Rb ratios have been used as evidence that fluids interact with altered basalt in some vent systems and fresh basalt in others (Palmer and Edmond, 1989). However, fluid reaction with altered basalt should express itself in both Li isotopes and Cs/Rb ratios given that all three elements leach similarly from the rock (Seyfried et al., 1998). Cs/Rb ratios may vary between vent sites as a result of processes such as differing Cs and Rb behavior during alteration above 400 °C (Volfinger, 1976; Berndt, 1987). Li, Rb, and Cs readily dissolve into hydrothermal fluid, leaving behind a rock depleted in these elements (Seyfried et al., 1998). The constant concentration of these three elements in vent fluids over time also demonstrates progressive infiltration of hydrothermal fluids into fresh basalt (Seyfried and Shanks, 2004). These data justify the use of δ^{44}Ca of unaltered MORB as the host rocks at EPR and JdFR.

As demonstrated by Amini et al. (2008), precipitation of anhydrite during mixing of seawater and hydrothermal fluid will fractionate Ca isotopes. This fractionation will undoubtedly sequester light Ca (relative to the mixed seawater-hydrothermal fluid) in the shallow ocean crust, thereby affecting the composition of Ca isotopes that reach the ocean. The extent to which anhydrite precipitation alters the hydrothermal fluid Ca isotope flux to the ocean will require quantification of the size and isotopic composition of the global anhydrite reservoir. It should be noted, however, that anhydrite precipitation during any type of mixing (and the resultant Ca isotope fractionation) does not alter the end member hydrothermal fluid δ^{44}Ca. By definition, the chemical and isotopic composition of an end member fluid (0 mM/kg Mg) results from fluid-mineral reactions and phase separation at depth before any mixing occurs (e.g. Bischoff and Seyfried, 1978; Von Damm et al., 1985). It is also not possible to precipitate anhydrite directly from end member fluid. Experiments, sulfur isotopes and analysis of drill core all indicate the presence of anhydrite at depth (Seyfried and Ding, 1995; Ono et al., 2007; Alt et al., 2010). Thus, end member fluids are anhydrite saturated at depth and become progressively under saturated as they rise and cool due to the retrograde solubility of anhydrite.

Further research is necessary in order to rigorously quantify the reactions that result in the observed δ^{44}Ca of MOR hydrothermal fluids. Of particular interest are measurements of Ca isotope systematics between plagioclase, diopside, epidote, and coexisting fluid. These three minerals are primary hosts for Ca in MORB and control the Ca concentrations of vent fluids (Berndt et al., 1988; Seyfried et al., 1988) and likely the fluid Ca isotopic signature. Non-zero equilibrium Ca isotope fractionation has been documented at 1000 °C between coexisting clinopyroxene-orthopyroxene (Huang et al., 2010; Feng et al., 2014), suggesting a similar pattern may exist between minerals and fluid in MOR hydrothermal systems. If non-zero equilibrium Ca isotope fractionation is confirmed, the lack of fractionation observed in MOR systems would be due to kinetic effects. Fluid residence times at temperatures above 200 °C have been estimated between 1 and 2 years at Main Endeavor Field, JdFR based on ^{228}Ra/^{226}Ra activity ratios (Kadko and Butterfield, 1998), whereas sulfur isotope systematics from EPR and Mid-Atlantic Ridge vent sites indicate fluids reside at temperatures above 400 °C for a maximum of several days (Ohmoto and Lasaga, 1982; Ono et al., 2007). Ca isotope disequilibrium is therefore possible given the time (minimum of 74 days) necessary to achieve 90% fluid-anhydrite Ca isotope exchange, as determined in the present study. Additionally, at 300 °C, a minimum of 200 years is necessary for O isotope equilibrium between NaCl fluids and aluminosilicate minerals (Cole et al., 1992). Given the similar rates of Ca and O isotope exchange between anhydrite and fluid (Fig. 7), the results of Cole et al. (1992) demonstrate that Ca isotope exchange between fluid and igneous minerals may be considerably slower than between anhydrite and dissolved Ca.

5. CONCLUSIONS

Phase separation experiments performed in the $CaSO_4$-NaCl-H_2O system indicate that there is insignificant Ca isotope fractionation between coexisting vapors and liquids at elevated temperatures and pressures. The rate data indicate that at 410 °C, 50 MPa a minimum of 74 days are necessary to achieve fluid-anhydrite Ca isotopic equilibrium. The data also show that at relatively constant SO_4 concentration the rate of Ca isotope exchange increases with higher total dissolved Ca, suggesting the importance of concentration on isotopic exchange in systems at chemical equilibrium. Applying the rate data to the phase separation experiments indicates that significant changes in the isotopic composition of either anhydrite or the vapor and liquid are unlikely with more reaction time.

End member fluid samples from basalt-hosted seafloor hydrothermal systems along the Juan de Fuca Ridge (Main Endeavor Field and Axial Volcano) and East Pacific Rise (9°50′N and 13°N) have δ^{44}Ca that range between −0.98 and −1.13‰ (SW). Within analytical error, there is no observable Ca isotope fractionation between end member fluid and host rock, MORB. Together, the phase separation experiments and vent fluids indicate that neither phase separation nor fluid-rock reactions at depth fractionate Ca isotopes in high temperature basalt-hosted vent systems.

ACKNOWLEDGEMENTS

We thank Rick Knurr (University of Minnesota), Elizabeth Lundstrom and Nic Slater (Princeton University) for analysis of both the experimental and vent fluid samples. Dr. Nicholas Seaton (Characterization Facility, University of Minnesota) provided assistance with the SEM. J.A. Higgins thanks the Princeton Environmental Institute (PEI) Grand Challenge Program for water-rock interactions. The authors also gratefully acknowledge funding provided by NSF grant OCE #1426695 (WES). Reviews from Shaun T. Brown and two anonymous referees greatly improved the quality of this contribution.

APPENDIX A. SUPPLEMENTARY MATERIAL

Supplementary data assocated with this article can be found, in the online version, at https://doi.org/10.1016/j.gca.2018.01.028.

REFERENCES

Alt J. C., Laverne C., Coggon R. M., Teagle D. A. H., Banerjee N. R., Morgan S., Smith-Duque C. E., Harris M. and Galli L. (2010) Subsurface structure of a submarine hydrothermal system in ocean crust formed at the East Pacific Rise, ODP/IODP Site 1256. *Geochem. Geophys. Geosyst.* **11**.

Amini M., Eisenhauer A., Böhm F., Fietzke J., Bach W., Garbe-Schönberg D., Rosner M., Bock B., Lackschewitz K. S. and Hauff F. (2008) Calcium isotope ($\delta^{44/40}$Ca) fractionation along hydrothermal pathways, Logatchev field (Mid-Atlantic Ridge, 14°45′N). *Geochim. Cosmochim. Acta* **72**, 4107–4122.

Amini M., Eisenhauer A., Böhm F., Holmden C., Kreissig K., Hauff F. and Jochum K. P. (2009) Calcium isotopes ($\delta^{44/40}$Ca) in MPI-DING reference glasses, USGS rock powders and various rocks: evidence for Ca isotope fractionation in terrestrial silicates. *Geostand. Geoanal. Res.* **33**, 231–247.

Anbar A. D., Jarzecki A. A. and Spiro T. G. (2005) Theoretical investigation of iron isotope fractionation between $Fe(H_2O)_6^{3+}$ and $Fe(H_2O)_6^{2+}$: implications for iron stable isotope geochemistry. *Geochim. Cosmochim. Acta* **69**, 825–837.

Antonelli M. A., Pester N. J., Brown S. T. and DePaolo D. J. (2017) Effect of paleoseawater composition on hydrothermal exchange in midocean ridges. PNAS, 201709145.

Berndt M. E. (1987) *Experimental and Theoretical Constraints on the Origin of Mid-Ocean Ridge Geothermal Fluids. PhD*. University of Minnesota.

Berndt M. E., Seyfried W. E. and Beck J. W. (1988) Hydrothermal alteration processes at midocean ridges: experimental and theoretical constraints from Ca and Sr exchange reactions and Sr isotopic ratios. *J. Geophys. Res.* **93**, 4573–4583.

Berndt M. E., Seal R. R., Shanks W. C. and Seyfried, Jr., W. E. (1996) Hydrogen isotope systematics of phase separation in submarine hydrothermal systems: experimental calibration and theoretical models. *Geochim. Cosmochim. Acta* **60**, 1595–1604.

Bethke C. (2008) Geochemical and Biogeochemical Reaction Modeling. Cambridge Press, Cambridge, U.K.

Bischoff J. L. and Seyfried W. E. (1978) Hydrothermal chemistry of seawater from 25 degrees to 350 degrees C. *Am. J. Sci.* **278**, 838–860.

Bischoff J. L., Rosenbauer R. J. and Pitzer K. S. (1986) The system NaCl-H_2O: relations of vapor-liquid near the critical temperature of water and of vapor-liquid-halite from 300 to 500 C. *Geochim. Cosmochim. Acta* **50**, 1437–1444.

Bischoff J. L. and Pitzer K. S. (1989) Liquid-vapor relations for the system NaCl-H_2O; summary of the P-T-x surface from 300 degrees to 500 degrees C. *Am. J. Sci.* **289**, 217–248.

Blättler C. L., Miller N. R. and Higgins J. A. (2015) Mg and Ca isotope signatures of authigenic dolomite in siliceous deep-sea sediments. *Earth Planet. Sci. Lett.* **419**, 32–42.

Bradley A. M., Feezor M. D., Singh H. and Sorrell F. Y. (2001) Power systems for autonomous underwater vehicles. *IEEE J. Oceanic Eng.* **26**, 526–538.

Brantley S. L., Kubicki J. D. and White A. F. (Eds.) (2008) Kinetics of Water-Rock Interaction. Springer, New York, NY.

Brown S. T., Kennedy B. M., DePaolo D. J., Hurwitz S. and Evans W. C. (2013) Ca, Sr, O and D isotope approach to defining the chemical evolution of hydrothermal fluids: example from Long Valley, CA, USA. *Geochim. Cosmochim. Acta* **122**, 209–225.

Bullen T. D., Kim S. and Paytan A. (2003) Ca isotope fractionation during Ca-carbonate precipitation: there's more to it than temperature. *Geochim. Cosmochim. Acta* **67**, A049.

Chacko T., Cole D. R. and Horita J. (2001) Equilibrium oxygen, hydrogen and carbon isotope fractionation factors applicable to geologic systems. In Stable Isotope Geochemistry Reviews in Mineralogy and Geochemistry. Mineralogical Society of America, Geochemical Society.

Chai B. (1975) The Kinetics and Mass Transfer of Calcite During Hydrothermal Recrystallization Process. PhD Thesis, Yale University.

Chan L. H., Edmond J. M., Thompson G. and Gillis K. (1992) Lithium isotopic composition of submarine basalts: implications for the lithium cycle in the oceans. *Earth Planet. Sci. Lett.* **108**, 151–160.

Chan L.-H., Edmond J. M. and Thompson G. (1993) A lithium isotope study of hot springs and metabasalts from Mid-Ocean Ridge Hydrothermal Systems. *J. Geophys. Res.* **98**, 9653–9659.

Chialvo A. A. and Horita J. (2009) Liquid-vapor equilibrium isotopic fractionation of water: how well can classical water models predict it?. *J. Chem. Phys.* **130** 094509.

Chiba H., Kusakabe M., Hirano S.-I., Matsuo S. and Somiya S. (1981) Oxygen isotope fractionation factors between anhydrite and water from 100 to 550 C. *Earth Planet. Sci. Lett.* **53**, 55–62.

Cole D. R., Ohmoto H. and Lasaga A. C. (1983) Isotopic exchange in mineral-fluid systems. I. Theoretical evaluation of oxygen isotopic exchange accompanying surface reactions and diffusion. *Geochim. Cosmochim. Acta* **47**, 1681–1693.

Cole D. R. (1992) Influence of solution composition and pressure on the rates of oxygen isotope exchange in the system: calcite/1bH2O/1bNaCl at elevated temperatures. *Chem. Geol.* **102**, 199–216.

Cole D. R., Ohmoto H. and Jacobs G. K. (1992) Isotopic exchange in mineral-fluid systems: III. Rates and mechanisms of oxygen isotope exchange in the system granite-$H_2O \pm NaCl \pm KCl$ at hydrothermal conditions. *Geochim. Cosmochim. Acta* **56**, 445–466.

Cole D. R. and Chakraborty S. (2001) Rates and mechanisms of isotopic exchange. In Stable Isotope Geochemistry (eds. J. W. Valley and D. R. Cole). Reviews in Mineralogy and Geochemistry. Mineralogical Society of America, Geochemical Society.

Colla C. A., Wimpenny J., Yin Q.-Z., Rustad J. R. and Casey W. H. (2013) Calcium-isotope fractionation between solution and solids with six, seven or eight oxygens bound to Ca(II). *Geochim. Cosmochim. Acta* **121**, 363–373.

Criss R. E., Gregory R. T. and Taylor H. P. (1987) Kinetic theory of oxygen isotopic exchange between minerals and water. *Geochim. Cosmochim. Acta* **51**, 1099–1108.

Criss R. E. (1999) Principles of Stable Isotope Distribution. Oxford University Press, Oxford.

De La Rocha C. L. and DePaolo D. J. (2000) Isotopic evidence for variations in the marine calcium cycle over the cenozoic. *Science* **289**, 1176–1178.

DePaolo D. (2004) Calcium isotopic variations produced by biological, kinetic, radiogenic and nucleosynthetic processes. In Geochemistry of non-traditional stable isotopes (eds. C. M. Johnson, B. L. Beard, and F. Albarede). Reviews in Mineralogy and Geochemistry.

DePaolo D. J. (2011) Surface kinetic model for isotopic and trace element fractionation during precipitation of calcite from aqueous solutions. *Geochim. Cosmochim. Acta* **75**, 1039–1056.

Driesner T. (2007) The system H_2O–NaCl. Part II: Correlations for molar volume, enthalpy, and isobaric heat capacity from 0 to 1000 C, 1 to 5000 bar, and 0 to 1 XNaCl. *Geochim. Cosmochim. Acta* **71**, 4902–4919.

Driesner T. and Heinrich C. A. (2007) The system H_2O–NaCl. Part I: Correlation formulae for phase relations in temperature–pressure–composition space from 0 to 1000 C, 0 to 5000 bar, and 0 to 1 XNaCl. *Geochim. Cosmochim. Acta* **71**, 4880–4901.

Fantle M. S. (2010) Evaluating the Ca isotope proxy. *Am. J. Sci.* **310**, 194–230.

Fantle M. S. and Tipper E. T. (2014) Calcium isotopes in the global biogeochemical Ca cycle: implications for development of a Ca isotope proxy. *Earth Sci. Rev.* **129**, 148–177.

Feng C., Qin T., Huang S., Wu Z. and Huang F. (2014) First-principles investigations of equilibrium calcium isotope fractionation between clinopyroxene and Ca-doped orthopyroxene. *Geochim. Cosmochim. Acta* **143**, 132–142.

Feng L., Zhou L., Yang L., DePaolo D. J., Tong S.-Y., Liu Y.-S., Owens T. L. and Gao S. (2017) Calcium isotopic compositions of sixteen USGS reference materials. *Geostand. Geoanal. Res.* **41**, 93–106.

Fontaine F. J., Wilcock W. S. D., Foustoukos D. E. and Butterfield D. A. (2009) A Si-Cl geothermobarometer for the reaction zone of high-temperature, basaltic-hosted mid-ocean ridge hydrothermal systems: Si/Cl-Inferred P-T In MOR hydrothermal systems. *Geochem. Geophys. Geosyst.* **10**.

Foustoukos D. I., James R. H., Berndt M. E. and Seyfried, Jr., W. E. (2004) Lithium isotopic systematics of hydrothermal vent fluids at the Main Endeavour Field, Northern Juan de Fuca Ridge. *Chem. Geol.* **212**, 17–26.

Foustoukos D. I. and Seyfried W. E. (2007a) Quartz solubility in the two-phase and critical region of the NaCl–KCl–H_2O system: implications for submarine hydrothermal vent systems at 9 50′N East Pacific Rise. *Geochim. Cosmochim. Acta* **71**, 186–201.

Foustoukos D. I. and Seyfried W. E. (2007b) Trace element partitioning between vapor, brine and halite under extreme phase separation conditions. *Geochim. Cosmochim. Acta* **71**, 2056–2071.

Foustoukos D. I., Pester N. J., Ding K. and Seyfried W. E. (2009) Dissolved carbon species in associated diffuse and focused flow hydrothermal vents at the Main Endeavour Field, Juan de Fuca Ridge: phase equilibria and kinetic constraints. *Geochem. Geophys. Geosyst.* **10**, Q10003.

Frierdich A. J., Beard B. L., Scherer M. M. and Johnson C. M. (2014) Determination of the Fe(II)aq–magnetite equilibrium iron isotope fractionation factor using the three-isotope method and a multi-direction approach to equilibrium. *Earth Planet. Sci. Lett.* **391**, 77–86.

Graham C. M. (1981) Experimental hydrogen isotope studies III: diffusion of hydrogen in hydrous minerals, and stable isotope exchange in metamorphic rocks. *Contr. Mineral. Petrol.* **76**, 216–228.

Handler R. M., Frierdich A. J., Johnson C. M., Rosso K. M., Beard B. L., Wang C., Latta D. E., Neumann A., Pasakarnis T., Premaratne W. A. P. J. and Scherer M. M. (2014) Fe(II)-catalyzed recrystallization of goethite revisited. *Environ. Sci. Technol.* **48**, 11302–11311.

Hardardóttir V., Brown K. L., Fridriksson T., Hedenquist J. W., Hannington M. D. and Thorhallsson S. (2009) Metals in deep liquid of the Reykjanes geothermal system, southwest Iceland: implications for the composition of seafloor black smoker fluids. *Geology* **37**, 1103–1106.

Hardie L. A. (1996) Secular variation in seawater chemistry: an explanation for the coupled secular variation in the mineralogies of marine limestones and potash evaporites over the past 600 m.y. *Geology* **24**, 279–283.

Heinrich C. A., Günther D., Audétat A., Ulrich T. and Frischknecht R. (1999) Metal fractionation between magmatic brine and vapor, determined by microanalysis of fluid inclusions. *Geology* **27**, 755–758.

Helgeson H. C. and Kirkham D. H. (1974) Theoretical prediction of the thermodynamic behavior of aqueous electrolytes at high pressures and temperatures; I, Summary of the thermodynamic/electrostatic properties of the solvent. *Am. J. Sci.* **274**, 1089–1198.

Helgeson H. C., Kirkham D. H. and Flowers G. C. (1981) Theoretical prediction of the thermodynamic behavior of aqueous electrolytes by high pressures and temperatures; IV, Calculation of activity coefficients, osmotic coefficients, and apparent molal and standard and relative partial molal properties to 600 degrees C and 5kb. *Am. J. Sci.* **281**, 1249–1516.

Holland H. D. (2005) Sea level, sediments and the composition of seawater. *Am. J. Sci.* **305**, 220–239.

Huang S., Farkaš J. and Jacobsen S. B. (2010) Calcium isotopic fractionation between clinopyroxene and orthopyroxene from mantle peridotites. *Earth Planet. Sci. Lett.* **292**, 337–344.

Husson J. M., Higgins J. A., Maloof A. C. and Schoene B. (2015) Ca and Mg isotope constraints on the origin of Earth's deepest C excursion. *Geochim. Cosmochim. Acta* **160**, 243–266.

Johnson, Oelkers and Helgeson (1992) SUPCRT92: a software package for calculating the standard molal thermodynamic properties of minerals, gases, aqueous species and reactions from 1 to 500 bar and 0 to 1000 C. *Comput. Geosci.* **18**, 899–947.

Johnson C. M., Skulan J. L., Beard B. L., Sun H., Nealson K. H. and Braterman P. S. (2002) Isotopic fractionation between Fe (III) and Fe(II) in aqueous solutions. *Earth Planet. Sci. Lett.* **195**, 141–153.

Johnson C. M., Beard B. L. and Albarede F. (2004) Overview and general concepts. *Rev. Mineral. Geochem.* **55**, 1–24.

Kadko D. and Butterfield D. A. (1998) The relationship of hydrothermal fluid composition and crustal residence time to maturity of vent fields on the Juan de Fuca Ridge. *Geochim. Cosmochim. Acta* **62**, 1521–1533.

Kiyosu Y. (1973) Sulfur isotopic fractionation among sphalerite, galena and sulfide ions. *Geochem. J.* **7**, 191–199.

Knauss K. G., Wolery T. J. and Jackson K. J. (1990) A new approach to measuring pH in brines and other concentrated electrolytes. *Geochim. Cosmochim. Acta* **54**, 1519–1523.

Kong X.-Z., Tutolo B. M. and Saar M. O. (2013) DBCreate: a SUPCRT92-based program for producing EQ3/6, TOUGHREACT, and GWB thermodynamic databases at user-defined T and P. *Comput. Geosci.* **51**, 415–417.

Kusakabe M. and Robinson B. W. (1977) Oxygen and sulfur isotope equilibria in the $BaSO_4$-HSO_4-H_2O system from 110 to 350 C and applications. *Geochim. Cosmochim. Acta* **41**, 1033–1040.

Lasaga A. C. (1981a) Rate laws of chemical reactions. In Kinetics of Geological Processes (eds. A. C. Lasaga and R. J. Kirkpatrick). Reviews in Mineralogy. Mineralogical Society of America. pp. 1–34.

Lasaga A. C. (1981b) The atomistic basis of kinetics: Defects in minerals. In Kinetics of Geological Processes (eds. A. C. Lasaga and R. J. Kirkpatrick). Reviews in Mineralogy. Mineralogical Society of America. pp. 261–320.

Lehn G. O. and Jacobson A. D. (2015) Optimization of a 48Ca–43Ca double-spike MC-TIMS method for measuring Ca isotope ratios (δ44/40Ca and δ44/42Ca): limitations from filament reservoir mixing. *J. Anal. At. Spectrom.* **30**, 1571–1581.

Liebscher A., Meixner A., Romer R. L. and Heinrich W. (2005) Liquid-vapor fractionation of boron and boron isotopes: experimental calibration at 400 C/23 MPa to 450 C/42 MPa. *Geochim. Cosmochim. Acta* **69**, 5693–5704.

Liebscher A., Barnes J. and Sharp Z. (2006) Chlorine isotope vapor–liquid fractionation during experimental fluid-phase separation at 400 C/23 MPa to 450 C/42 MPa. *Chem. Geol.* **234**, 340–345.

Lowell R. P., Yao Y. and Germanovich L. N. (2003) Anhydrite precipitation and the relationship between focused and diffuse flow in seafloor hydrothermal systems. *J. Geophys. Res.* **108**, 2424.

Marriott C. S., Henderson G. M., Belshaw N. S. and Tudhope A. W. (2004) Temperature dependence of δ7Li, δ44Ca and Li/Ca during growth of calcium carbonate. *Earth Planet. Sci. Lett.* **222**, 615–624.

McDermott J. (2015) Geochemistry of deep-sea hydrothermal vents fluids from the Mid-Cayman Rise, Caribbean sea. PhD, WHOI/MIT.

Ohmoto H. and Lasaga A. C. (1982) Kinetics of reactions between aqueous sulfates and sulfides in hydrothermal systems. *Geochim. Cosmochim. Acta* **46**, 1727–1745.

Ono S., Shanks, III, W. C., Rouxel O. J. and Rumble D. (2007) S-33 constraints on the seawater sulfate contribution in modern seafloor hydrothermal vent sulfides. *Geochim. Cosmochim. Acta* **71**, 1170–1182.

Palache C., Berman H. and Frondel C. (1951) *The System of Mineralogy*, 7th ed. John Wiley & Sons, New York.

Palmer M. R. and Edmond J. M. (1989) Cesium and rubidium in submarine hydrothermal fluids: evidence for recycling of alkali elements. *Earth Planet. Sci. Lett.* **95**, 8–14.

Pester N. J., Rough M., Ding K. and Seyfried W. E. (2011) A new Fe/Mn geothermometer for hydrothermal systems: implications for high-salinity fluids at 13 N on the East Pacific Rise. *Geochim. Cosmochim. Acta* **75**, 7881–7892.

Pester N. J., Ding K. and Seyfried W. E. (2014) Magmatic eruptions and iron volatility in deep-sea hydrothermal fluids. *Geology* **42**, 255–258.

Pester N. J., Ding K. and Seyfried, Jr., W. E. (2015) Vapor–liquid partitioning of alkaline earth and transition metals in NaCl-dominated hydrothermal fluids: an experimental study from 360 to 465 C, near-critical to halite saturated conditions. *Geochim. Cosmochim. Acta* **168**, 111–132.

Pokrovski G. S., Roux J. and Harrichoury J.-C. (2005) Fluid density control on vapor-liquid partitioning of metals in hydrothermal systems. *Geology* **33**, 657–660.

Pokrovski G., Borisova A. and Bychkov A. (2013) Speciation and transport of metals and metalloids in geological vapors. In Thermodynamics of Geothermal Fluids (eds. A. Stefansson, T. Driesner, and P. Benezeth). Reviews in Mineralogy and Geochemistry. Mineralogical Society of America, Geochemical Society.

Rempel K. U., Liebscher A., Meixner A., Romer R. L. and Heinrich W. (2012) An experimental study of the elemental and isotopic fractionation of copper between aqueous vapour and liquid to 450 C and 400 bar in the CuCl–NaCl–H_2O and CuCl–NaHS–NaCl–H_2O systems. *Geochim. Cosmochim. Acta* **94**, 199–216.

Rouxel O., Fouquet Y. and Ludden J. N. (2004) Copper isotope systematics of the Lucky Strike, Rainbow, and Logatchev sea-floor hydrothermal fields on the Mid-Atlantic Ridge. *Econ. Geol.* **99**, 585–600.

Rouxel O., Shanks, III, W. C., Bach W. and Edwards K. J. (2008) Integrated Fe- and S-isotope study of seafloor hydrothermal vents at East Pacific Rise 9–10 N. *Chem. Geol.* **252**, 214–227.

Rustad J. R., Casey W. H., Yin Q.-Z., Bylaska E. J., Felmy A. R., Bogatko S. A., Jackson V. E. and Dixon D. A. (2010) Isotopic fractionation of Mg^{2+}(aq), Ca^{2+}(aq), and Fe^{2+}(aq) with carbonate minerals. *Geochim. Cosmochim. Acta* **74**, 6301–6323.

Schiller M., Paton C. and Bizzarro M. (2012) Calcium isotope measurement by combined HR-MC-ICPMS and TIMS. *J. Anal. At. Spectrom.* **27**, 38–49.

Schmitt A.-D., Chabaux F. and Stille P. (2003) The calcium riverine and hydrothermal isotopic fluxes and the oceanic calcium mass balance. *Earth Planet. Sci. Lett.* **213**, 503–518.

Seewald J. S., Doherty K. W., Hammar T. R. and Liberatore S. P. (2002) A new gas-tight isobaric sampler for hydrothermal fluids. *Deep Sea Res. Part I* **49**, 189–196.

Seyfried W. E. Jr., Janecky, D.R. and Berndt, M.E. (1987) Rocking autoclaves for hydrothermal experiments II: The flexible cell system. In Experimental Hydrothermal Techniques (eds. Ulmer, G. and Barnes, H.). Wiley Interscience. pp. 216–240.

Seyfried W. E., Berndt M. E. and Seewald J. S. (1988) Hydrothermal alteration processes at mid-ocean ridges; constraints from diabase alteration experiments, hot spring fluids and composition of the oceanic crust. *Can Mineral* **26**, 787–804.

Seyfried W. and Ding K. (1995) Phase equilibria in subseafloor hydrothermal systems: a review of the role of redox, temperature, pH and dissolved Cl on the chemistry of hot spring fluids at mid-ocean ridges. In Seafloor Hydrothermal Systems: Physical, Chemical Biological, and Geological Interactions Geophysical Monograph 91. American Geophysical Union. pp. 248–272.

Seyfried W. E., Chen X. and Chan L.-H. (1998) Trace element mobility and lithium isotope exchange during hydrothermal alteration of seafloor weathered basalt: an experimental study at 350 C, 500 bars. *Geochim. Cosmochim. Acta* **62**, 949–960.

Seyfried W. E., Seewald J. S., Berndt M. E., Ding K. and Foustoukos D. I. (2003) Chemistry of hydrothermal vent fluids from the Main Endeavour Field, northern Juan de Fuca Ridge: geochemical controls in the aftermath of June 1999 seismic events. *J. Geophys. Res.* **108**, 2429.

Seyfried W. E. and Shanks W. C. (2004) Alteration and mass transport in mid-ocean ridge hydrothermal systems: controls on the chemical and isotopic evolution of high-temperature crustal fluids. *Hydrogeol. Ocean. Lithosphere* **1**, 451.

Simmons S. F. and Brown K. L. (2006) Gold in magmatic hydrothermal solutions and the rapid formation of a giant ore deposit. *Science* **314**, 288–291.

Sleep N. H. (1991) Hydrothermal circulation, anhydrite precipitation, and thermal structure at ridge axes. *J. Geophys. Res.* **96**, 2375–2387.

Sourirajan S. and Kennedy G. C. (1962) The system H_2O-NaCl at elevated temperatures and pressures. *Am. J. Sci.* **260**, 115–141.

Syverson D. D., Pester N. J., Craddock P. R. and Seyfried, Jr., W. E. (2014) Fe isotope fractionation during phase separation in the NaCl–H_2O system: an experimental study with implications for seafloor hydrothermal vents. *Earth Planet. Sci. Lett.* **406**, 223–232.

Syverson D. D., Ono S., Shanks W. C. and Seyfried, Jr., W. E. (2015) Multiple sulfur isotope fractionation and mass transfer processes during pyrite precipitation and recrystallization: an experimental study at 300 and 350 C. *Geochim. Cosmochim. Acta* **165**, 418–434.

Tang J., Dietzel M., Böhm F., Köhler S. J. and Eisenhauer A. (2008) Sr^{2+}/Ca^{2+} and $^{44}Ca/^{40}Ca$ fractionation during inorganic calcite formation: II. Ca isotopes. *Geochim. Cosmochim. Acta* **72**, 3733–3745.

Tanger J. C. and Helgeson H. C. (1988) Calculation of the thermodynamic and transport properties of aqueous species at high pressures and temperatures; revised equations of state for the standard partial molal properties of ions and electrolytes. *Am. J. Sci.* **288**, 19–98.

Tivey M. K., Humphris S. E., Thompson G., Hannington M. D. and Rona P. A. (1995) Deducing patterns of fluid flow and mixing within the TAG active hydrothermal mound using mineralogical and geochemical data. *J. Geophys. Res.* **100**, 12527–12555.

Valdes M. C., Moreira M., Foriel J. and Moynier F. (2014) The nature of Earth's building blocks as revealed by calcium isotopes. *Earth Planet. Sci. Lett.* **394**, 135–145.

Volfinger M. (1976) Effet de la temperature sur les distributions de sodium, rubidium et cesium entre la sanidine, la muscovite, la phologpite, et une solution hydrothermale sours une pression de 1 kbar. *Geochim. Cosmochim. Acta* **40**, 267–282.

Von Damm K. L., Edmond J. M., Grant B., Measures C. I., Walden B. and Weiss R. F. (1985) Chemistry of submarine hydrothermal solutions at 21 N, East Pacific Rise. *Geochim. Cosmochim. Acta* **49**, 2197–2220.

Von Damm K. L. (1995) Controls on the chemistry and temporal variability of seafloor hydrothermal fluids. *Seafloor Hydrothermal Syst.: Phys., Chem., Biol., Geol. Interact.*, 222–247.

Von Damm K. L. (2004) Evolution of the hydrothermal system at East Pacific Rise 9°50′N: geochemical evidence for changes in the upper oceanic crust. In Mid-Ocean Ridges (eds. C. R. German, J. Lin, and L. M. Parson). American Geophysical Union. pp. 285–304. Available at: <http://onlinelibrary.wiley.com/doi/10.1029/148GM12/summary> [Accessed June 17, 2016].

Wombacher F., Eisenhauer A., Heuser A. and Weyer S. (2009) Separation of Mg, Ca and Fe from geological reference materials for stable isotope ratio analyses by MC-ICP-MS and double-spike TIMS. *J. Anal. At. Spectrom.* **24**, 627–636.

Wu S. J., Yang C. J., Pester N. J. and Chen Y. (2011) A new hydraulically actuated titanium sampling valve for deep-sea hydrothermal fluid samplers. *IEEE J. Oceanic Eng.* **36**, 462–469.

Zhu P. and Macdougall J. D. (1998) Calcium isotopes in the marine environment and the oceanic calcium cycle. *Geochim. Cosmochim. Acta* **62**, 1691–1698.

Associate editor: Rachael James